OUKA
The University of Osaka
Institutional Knowledge Archive

Title	Impact of a small ellipticity on the sustainability condition of developed turbulence in a precessing spheroid
Author(s)	Horimoto, Yasufumi; Simonet-Davin, Gabriel; Katayama, Atsushi et al.
Citation	Physical Review Fluids. 2018, 3(4), p. 044603
Version Type	VoR
URL	https://hdl.handle.net/11094/100047
rights	Copyright 2018 by the American Physical Society
Note	

The University of Osaka Institutional Knowledge Archive : OUKA

https://ir.library.osaka-u.ac.jp/

The University of Osaka

Impact of a small ellipticity on the sustainability condition of developed turbulence in a precessing spheroid

Yasufumi Horimoto, Gabriel Simonet-Davin, Atsushi Katayama, and Susumu Goto
Graduate School of Engineering Science, Osaka University, 1-3 Machikaneyama, Toyonaka, Osaka 560-8531, Japan

(Received 16 October 2017; published 9 April 2018)

We experimentally investigate the flow transition to developed turbulence in a precessing spheroid with a small ellipticity. Fully developed turbulence appears through a subcritical transition when we fix the Reynolds number (the spin rate) and gradually increase the Poincaré number (the precession rate). In the transitional range of the Poincaré number, two qualitatively different turbulent states (i.e., fully developed turbulence and quiescent turbulence with a spin-driven global circulation) are stable and they are connected by a hysteresis loop. This discontinuous transition is in contrast to the continuous transition in a precessing sphere, for which neither bistable turbulent states nor hysteresis loops are observed. The small ellipticity of the container makes the global circulation of the confined fluid more stable, and it requires much stronger precession of the spheroid, than a sphere, for fully developed turbulence to be sustained. Nevertheless, once fully developed turbulence is sustained, its flow structures are almost identical in the spheroid and sphere. The argument [Lorenzani and Tilgner, J. Fluid Mech. **492**, 363 (2003); Noir *et al.*, Geophys. J. Int. **154**, 407 (2003)] on the basis of the analytical solution [Busse, J. Fluid Mech. **33**, 739 (1968)] of the steady global circulation in a weak precession range well describes the onset of the fully developed turbulence in the spheroid.

DOI: 10.1103/PhysRevFluids.3.044603

I. INTRODUCTION

It is incredibly difficult to predict the flow state of a fluid confined in a precessing container (Fig. 1) despite the simple motion of the container itself. One of the most remarkable features of the flow in a precessing cavity is that a weak precession can sustain fully developed turbulence [1]. This feature is attractive from geophysical (recall that the spin axis of the Earth is slowly precessing with a period of 26 000 years), engineering, and scientific points of view and many studies have been made [2–11]. Even recently, direct numerical simulations (DNSs) [12–20] and laboratory experiments [21–25], including the DRESDYN project [26–28], have been conducted to investigate the statistics and dynamics of turbulence in precessing cavities with different shapes (sphere, spheroid, cylinder, spherical shell, and spheroidal shell). Although developed turbulence in a precessing spheroid was discovered about 60 years ago [1], even the accurate condition that the developed turbulence is sustained in a precessing container is unknown. This is due to a nontrivial effect of the cavity shape on this strongly nonlinear problem. The shape effect was reported in the very first experimental study by Malkus [1], but it will be shown in much more detail in the rest of the present article. In the present study, we experimentally investigate the route to fully developed turbulence in a precessing spheroid with a small ellipticity (Fig. 1) and compare it with the laminar-turbulent transition in a precessing sphere to show that the small ellipticity has a substantial effect on the transition, although sustained developed turbulence is almost identical in these cavities.

 ©2018 American Physical Society

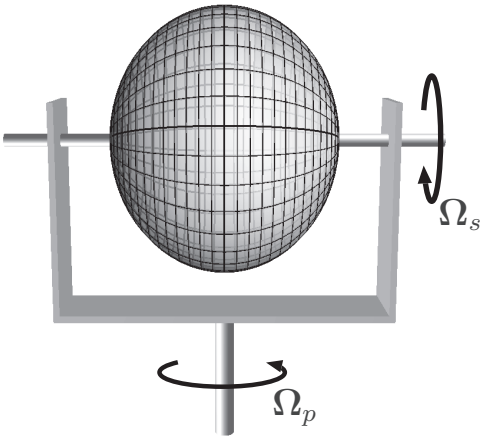

FIG. 1. A precessing oblate spheroid with ellipticity 0.1. We drive the precession by spinning, with an angular velocity $\mathbf{\Omega}_s$, the container on a turntable rotating with $\mathbf{\Omega}_p$. The minor axis of the spheroid is parallel to the spin axis and the two axes are perpendicular ($\mathbf{\Omega}_s \perp \mathbf{\Omega}_p$).

An advantage of this flow system is that, once we fix the cavity shape and the angle between the two axes of the rotations, only two nondimensional parameters,

$$\mathrm{Re} = \frac{a^2\Omega_s}{\nu} \quad \text{(Reynolds number)} \tag{1}$$

and

$$\mathrm{Po} = \frac{\Omega_p}{\Omega_s} \quad \text{(Poincaré number)}, \tag{2}$$

control flow states. Here, Ω_s and Ω_p are the amplitudes of the spin and precession angular velocities, respectively (Fig. 1). The kinematic viscosity of the confined fluid is denoted by ν and a is the equatorial radius of the cavity.

In our previous studies [23,24] on the flow in a precessing sphere, it was shown that the flow state drastically changed as Po increased for a fixed Re. (i) The confined fluid rotates at $\mathbf{\Omega}_s$ together with the cavity when $\mathrm{Po} = 0$. (ii) For a very weak precession, steady flow dominated by a simple circulation is sustained. The axis of this circulation is inclined with respect to the spin axis due to the Coriolis force. More precisely, the flow is steady in the frame rotating with $\mathbf{\Omega}_p$. This rotating frame is sometimes called the precession frame, and all of our experimental results are represented in this frame. Note that both the boundary condition and the inertial force (i.e., the Coriolis force) are time independent in the precession frame. (iii) This steady flow becomes unstable at a critical Poincaré number $\mathrm{Po}^{(c)}$, which depends on Re, and periodic flow is sustained in the cavity. (iv) For an intermediate but relatively weak precession range, i.e., $\mathrm{Po} = O(0.1)$, developed turbulence is sustained. (v) However, stronger precession ($\mathrm{Po} \gtrsim 0.2$) weakens the turbulence in a central region of the cavity. This is because the precession angular velocity vector $\mathbf{\Omega}_p$ is stationary in the laboratory frame, (vi) and, for further higher Po, it leads to steady flow. This steady flow, in the precession frame, is almost at rest except in the vicinity of the cavity wall, which rotates at $\mathbf{\Omega}_s$.

We also investigated the flow dependence on the small change of the cavity shape and observed that the Po dependence, summarized in the above paragraph, of flow in a precessing sphere was roughly similar even for a prolate spheroid with a small ellipticity [24]. Very interestingly, however, the condition to sustain unsteady flow significantly depends on the slight change of the cavity shape. More concretely, the critical Poincaré number $\mathrm{Po}^{(c)}$ at which the first bifurcation from steady to periodic flows occurs [(iii) in the previous paragraph] strongly depends on the cavity shape: $\mathrm{Po}^{(c)}$ is much larger for slightly prolate or oblate spheroids (with the ellipticity η being $-1/9$ and $1/10$,

respectively) than for a sphere [29]. Here, we define the ellipticity by

$$\eta = (a - b)/a, \tag{3}$$

where a is the radius of the circular cross section on the equatorial plane and b is the distance between the equatorial plane and the poles of the spheroidal cavity. For example, at $\mathrm{Re} = 4.0\times10^4$,

$$0.0047 < \mathrm{Po}^{(c)} < 0.0048 \tag{4}$$

for a sphere, whereas

$$0.0422 < \mathrm{Po}^{(c)} < 0.0425 \tag{5}$$

for the oblate spheroid with $\eta = 0.1$. Note that $\mathrm{Po}^{(c)}$ is about ten times larger for the spheroid than the sphere at this Re. Since an asymmetric cavity can drive flow of a confined fluid by the wall-normal stress, this may be counterintuitive but is explained by a stability analysis [18,29].

Although these recent studies have revealed the conditions for which unsteady flows are sustained in a sphere and spheroids, they cannot show the condition for developed turbulence to be sustained. We reemphasize that this condition is crucial for engineering applications of this system and important from the geophysical point of view. The concrete purpose of the present study is thus to experimentally reveal the precise route from unsteady flow to turbulence in the precessing oblate spheroid with a small ellipticity ($\eta = 0.1$) and show the difference from the route for a precessing sphere. We will also show the similarity of developed turbulence sustained in the spheroid and sphere.

To precisely describe the route to turbulence is, in general, a challenging problem. Even the longest standing problem of the laminar-turbulent transition in a pipe is still extensively investigated (see Ref. [30] for a recent breakthrough). The difficulty is due to complex bifurcations including subcritical transitions, which require nonlinear stability analysis. It is interesting to observe, in this context, that there exist bistable turbulent states in many rotating systems such as the Taylor-Couette flow [31,32], the spherical Couette flow [33], and forced rotating turbulence in a periodic cube [34]. Although it is known that this is also the case for precession-driven flows in a spheroid [1], a spheroidal shell [14], and a cylinder [28], no systematic study has been conducted to reveal the precise route to turbulence through the subcritical transition of the precessional flow. We therefore conduct careful laboratory experiments by using flow visualizations and particle image velocimetry (PIV) so that we can precisely describe the route to fully developed turbulence and its flow structures in the precessing spheroid. We will show, in the rest of the present article, that two stable turbulent states coexist for a given set of the parameters (Re,Po) in the transitional regime. One state originates from a steady spin-driven global rotational flow observed for lower Po and the other is the fully developed turbulence which is observed only for $\mathrm{Po} = O(0.1)$. These two turbulent states are connected by a hysteresis loop. However, neither such bistable turbulent states nor hysteresis loops are observed in a precessing sphere. These nontrivial observations are qualitatively explained by an argument suggested in Refs. [14,35] on the basis of the theory by Busse [36] for steady precessional flow.

II. EXPERIMENTAL SETUP

Since the details of the experimental setup (Fig. 2) are given in Refs. [24,25], here we briefly describe the setup. A stepper motor drives the spin $\mathbf{\Omega}_s$ of a cylindrical acrylic container with a spheroidal or spherical cavity on a turntable, which is rotated with $\mathbf{\Omega}_p$ by another stepper motor. A laser sheet, which rotates with the turntable, runs on the equatorial plane of the cavity and flow is recorded by a digital camera fixed on the turntable through the flat bottom window of the container. We use aluminum reflective flakes for flow visualizations (Figs. 3 and 8) and nylon powders with radius of about 50 μm for PIV. We conduct the PIV analysis by our own code, where the direct correlation algorithm is used.

We use two kinds of containers. One is with a spherical cavity with radius $a = 90$ mm, and the other is with an oblate spheroidal cavity ($a = 90$ mm and $b = 81$ mm). The minor radius of the spheroid is set to be parallel to the spin axis.

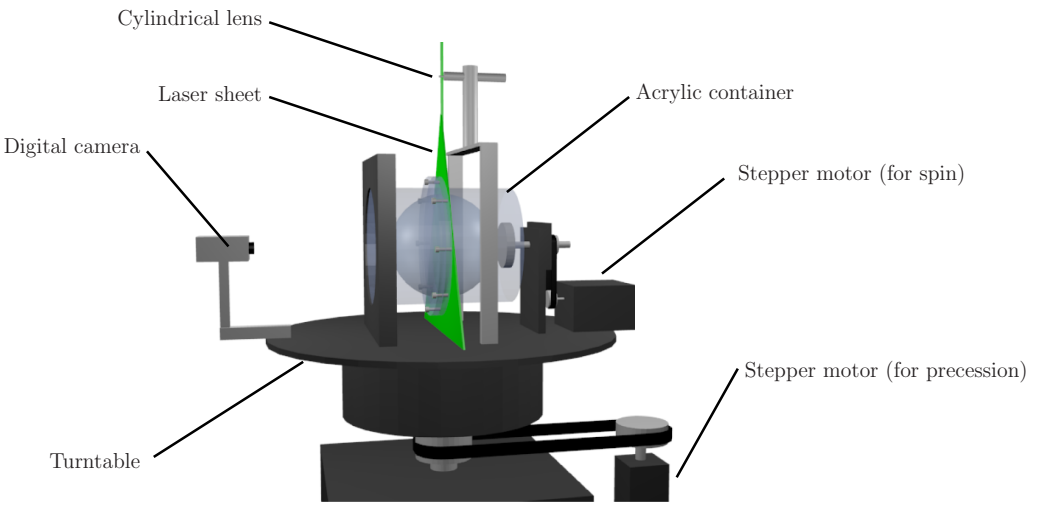

FIG. 2. Experimental apparatus. An acrylic cylindrical container with a spheroidal or spherical cavity spins (with the angular velocity $\mathbf{\Omega}_s$) on a turntable which rotates with $\mathbf{\Omega}_p$. A laser sheet, which rotates together with the turntable, for flow visualization and PIV is always on the equatorial plane of the cavity. Visualized flow is recorded by a camera fixed on the turntable.

As emphasized in the introduction, an advantage of the present system is that we can precisely control the experimental conditions. For this, we only need precisely set the two control parameters Re and Po defined by Eqs. (1) and (2), respectively. Since it is easy to accurately control the angular velocities Ω_s and Ω_p by using the stepper motors with small step angles, we only have to carefully control fluid temperature, on which ν depends. As described in Ref. [25], we surround the apparatus by thermal insulators and set an air conditioner for the space surrounding the apparatus in order to accurately (within 0.1 K during experiments) control the temperature of the working fluid.

The protocol of experiments is crucial for the following arguments. We fix Re and change Po in each series of experiments. In practice, we keep the magnitude Ω_s of the spin angular velocity of the container and change the magnitude Ω_p of the angular velocity of the turntable by steps. More concretely, we start with a sufficiently low (for the increasing Po experiments) or high (for decreasing Po experiments) Poincaré number, $\mathrm{Po}^{(0)}$, and change Po by steps with an increment of $\Delta\mathrm{Po}$. We set the increment $|\Delta\mathrm{Po}| = 0.0025$ in the transitional range and 0.01 in other ranges. For each parameter, we wait for 1000 spin periods before judging the flow state (in visualizations) or recording flow (for PIV) for the duration of 200 spin periods.

III. RESULTS

A. Two turbulent states

For $\mathrm{Re} = 4.0\times10^4$, unsteady flow is sustained in the oblate spheroid when the Poincaré number is larger than about 0.042 [see Eq. (5)]. The steady flow becomes unstable due to a parametric instability [18,37] at the critical Poincaré number $\mathrm{Po}^{(c)}$ ($\approx$0.042) and periodic flow just above $\mathrm{Po}^{(c)}$ is accompanied by a strong global circulation about an axis approximately perpendicular to the equatorial plane [23,24]. Here, the words *global circulation* denote the mean flow structure with almost uniform vorticity. This global circulation, which is as fast as the cavity wall $a\Omega_s$, originates from the solid-body rotation about the spin axis at $\mathrm{Po} = 0$. When we increase Po for the fixed Re, the flow gradually becomes turbulent. The flake visualization of the turbulence for $\mathrm{Po} = 0.055$ is shown in Fig. 3(a). This turbulence is also dominated by a global circulation about an axis which inclines from the spin axis [see the Supplemental Material [38] and Fig. 4(a), below] due to the Coriolis force.

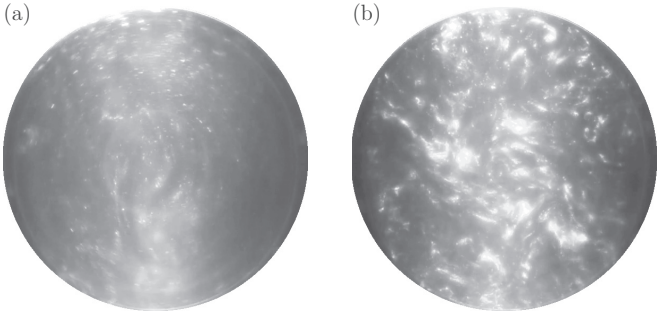

FIG. 3. Flow visualizations by using reflective flakes of two turbulent states in the oblate spheroid at a common set of parameters ($\mathrm{Re} = 4.0\times10^4$ and $\mathrm{Po} = 0.055$). (a) Quiescent turbulence, which is dominated by a spin-driven global circulation. (b) Developed turbulence. Movies are available in the Supplemental Material [38].

There are no small-scale turbulent eddies in this turbulence, and we call this flow state the quiescent turbulence (QT). Here, we call this flow *turbulence* simply because it is neither steady nor periodic, although it is far from fully developed turbulence. In other words, the QT is in the nonlinear regime defined in Ref. [28].

On the other hand, when we set the Poincaré number at a sufficiently large value, $\mathrm{Po} \approx 0.1$, developed turbulence is sustained in the cavity. The mean flow of this turbulence is nontrivial and it is

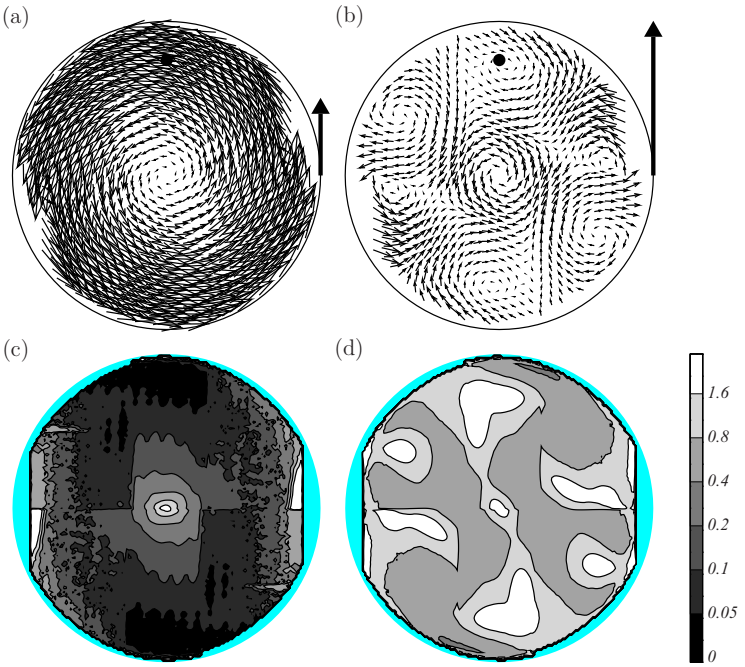

FIG. 4. [(a), (b)] Mean velocity and [(c), (d)] turbulence intensity on the equatorial plane evaluated by the PIV over 200 spin periods. The parameters are same as in Fig. 3: $\mathrm{Re} = 4.0\times10^4$ and $\mathrm{Po} = 0.055$. We observe [(a), (c)] QT and [(b), (d)] DT. The vertical arrow in panels (a) and (b) indicates the wall spin velocity $a\Omega_s$. The turbulence intensity in panels (c) and (d) is defined by the rms value of a velocity component normalized by the magnitude of the local mean velocity. The region where PIV data are absent is shaded in light blue in panels (c) and (d). The dot in panels (a) and (b) indicates the location for U_x to be calculated in Fig. 7.

not a simple global rotation about an axis (see the Supplemental Material [38]). We will quantitatively verify this important feature in the discussions on Figs. 4 and 9, below. It is interesting to observe that when we gradually decrease Po from Po ≈ 0.1 for the fixed Re, the developed turbulence is sustained even for Po exactly same as in Fig. 3(a); that is, Po $= 0.055$. The evidence is given in Fig. 3(b), where we observe small-scale turbulent eddies. This state is obviously different from the QT and is called the developed turbulence (DT) in the following. The difference is obvious in the Supplemental Material [38]. Namely, the flake pattern of the QT is globally circulating in a simple way, whereas the pattern of the DT moves in a complex way. We can also see the difference in the still images (Fig. 3): the flake pattern is finer and more complex in the DT, reflecting the existence of smaller scale eddies.

To quantitatively verify the difference between the two turbulent states visualized in Fig. 3, we show the results of PIV in Fig. 4. Figures 4(a) and 4(b) show the temporally averaged velocity field $\boldsymbol{U}$ on the equatorial plane, and Figs. 4(c) and 4(d) show the turbulence intensity on the plane. The wall speed ($a\Omega_s$) on the plane is indicated by the vertical arrow in Figs. 4(a) and 4(b), and the turbulence intensity is defined by $\sqrt{{u'_x}^2 + {u'_y}^2}/\sqrt{U_x^2 + U_y^2}$ with u'_x and u'_y being the rms values of the horizontal and vertical velocity components on the equatorial plane, respectively.

We observe clear differences between the two turbulent states in their mean velocity fields. The mean velocity of the QT [Fig. 4(a)] is dominated by a spin-driven global circulation, whereas the mean velocity of the DT [Fig. 4(b)] is complex with some vortices. More concretely, the mean flow of the QT is nearly uniform vorticity flow, which may be approximated by Eq. (6), whereas the mean flow of the DT is far from such a simple circulation. It is important to emphasize that the observed mean velocity field [Fig. 4(b)] of the DT is similar to the one observed in a precessing sphere (see Sec. III D for more detailed arguments) at similar Po. Since our DNS [20] showed that the mean flow of the DT in a precessing sphere was cavity-size complex-shaped vortices, we may conclude that the six vortices observed in the mean field [Fig. 4(b)] are the cross sections of these nontrivial vortical structures. This implies that the turbulence observed after the transition (see Sec. III C) is qualitatively different from the QT.

Because the QT seems to be continuously connected to the periodic flow, which stems from uniform vorticity flow by the parametric instability of inertial modes, and because the mean flow of the QT is approximately uniform vorticity flow, the origin of the QT is likely to be described in terms of nonlinear interactions of inertial modes superimposed on the uniform vorticity flow. However, concerning the DT, although we showed that the cavity-scale vortices sustained the small-scale turbulent eddies [25], it is unknown how these complex large-scale structures are created by a sufficiently strong precession to destroy the spin-driven global circulation. It is therefore hard to describe the origin of the DT.

It is also remarkable that the mean velocity in the QT is in the same order as the wall speed ($a\Omega_s$) whereas the mean velocity magnitudes in the DT are much smaller than those in the QT. Note the difference in the normalization of the length of the arrows in Figs. 4(a) and 4(b). Thus, the turbulence intensity, which is defined by using the local mean velocity magnitude, has much higher values in the DT [Fig. 4(d)] than in the QT [Fig. 4(c)]. The magnitudes of fluctuation velocity of the QT are less than about 20 percents of the mean velocity except around the center of the cavity where the mean velocity magnitude is small, whereas those in the DT are significantly larger than the QT in the entire space of the cavity. These observations are consistent with the flake visualizations in Fig. 3, which show that the QT has no significant fluctuations, whereas the DT is accompanied by significant fluctuations and smaller scale turbulent eddies.

B. Range of Po for the bistable states

In this subsection, we investigate the range of Po where the bistable turbulent states exist. We conduct similar experiments to the one described in the preceding subsection for seven different values of the Reynolds number: Re $= 1.0\times10^4$, 1.5×10^4, 2.0×10^4, 3.0×10^4, 4.0×10^4, 6.0×10^4, and 8.0×10^4. For each Re, the maximum value of Po for which the QT is sustained, when we increase

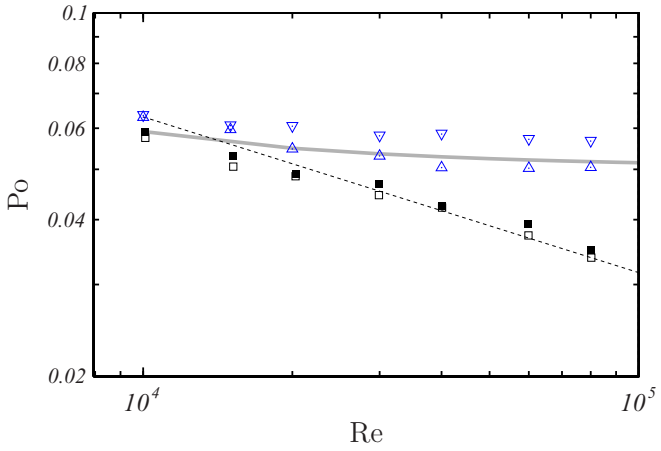

FIG. 5. The downward triangles (▽) denote the maximum Po for QT to be sustained when we increase Po for a given Re, while the upward triangles (△) denote the minimum Po for DT to be sustained when we decrease Po. These are plotted on the basis of visualizations of flow in the oblate spheroid. The gray curve denotes $\mathrm{Po}^{(t)}$ at which the inclination angle φ (Fig. 6) of the steady spin-driven global circulation becomes a decreasing function of Po for a fixed Re. For comparison, the maximum Po for steady flows and the minimum Po for periodic flows are plotted as a function of Re by open and closed squares [29], respectively. The dashed line indicates the scaling $\mathrm{Po} \propto \mathrm{Re}^{-3/10}$.

Po, for the duration of at least 1000 spin periods is plotted with a downward triangle in Fig. 5; while the minimum value of Po for which the DT is sustained over 1000 spin periods, when we decrease Po, is plotted with an upward triangle. Since the two turbulent states are quite different (Fig. 3), they are easily recognized by flake visualization. We may therefore plot Fig. 5 unambiguously on the basis of the flow visualizations.

Figure 5 shows that the range of Po (i.e., the range between the upward and downward triangles for a given Re) for the bistable turbulent states to be observed only weakly depends on Re. This is in contrast to the critical Poincaré number $\mathrm{Po}^{(c)}$ of the instability of steady flow depends on Re as $\mathrm{Po}^{(c)} \propto \mathrm{Re}^{-3/10}$ in the Re range shown in Fig. 5. To show this contrast, the data taken from Ref. [29] are also plotted in Fig. 5. We plot the maximum (□) and minimum (■) Po for which steady and unsteady flows are respectively observed in the oblate spheroid. It is clear that $\mathrm{Po}^{(c)}$ for the linear instability of steady flow rapidly decreases with Re, while the Poincaré number for the DT to be sustained seems to tend to a constant for $\mathrm{Re} \to \infty$. This implies that the range of the QT expands for higher Re. Recall here that QT is sustained in the range between the closed squares and the downward triangles in Fig. 5. However, the width of the Po range for the DT is more important for engineering applications as well as for the geophysics. The present results imply that the Poincaré number as high as $\mathrm{Po} \gtrsim 0.05$ is needed for the DT to be sustained in the spheroid. For $\mathrm{Po} \gtrsim 0.2$, on the other hand, the DT is significantly weakened in a central columnar region along the precession axis because of the stationary system rotation ($\mathbf{\Omega}_p$) about the precession axis fixed in the laboratory. In other words, the Po range for the DT in the oblate spheroid with the small ellipticity ($\eta = 0.1$) is limited for the examined Reynolds number ($10^4 \lesssim \mathrm{Re} \lesssim 10^5$) and it seems not to expand for higher Re.

For more quantitative arguments on the range of Po in which DT is sustained, we recall that the QT is accompanied by a spin-driven global circulation. Busse [36] analytically derived the steady circulation in the low-Po range by considering the torque balance, and, recently, Cébron *et al.* [39] and Noir and Cébron [40] extended his theory to flows in precessing triaxial ellipsoids. Using (3.19) in Ref. [36], we can express the magnitude ω (normalized by Ω_s) and the angle φ from the spin axis

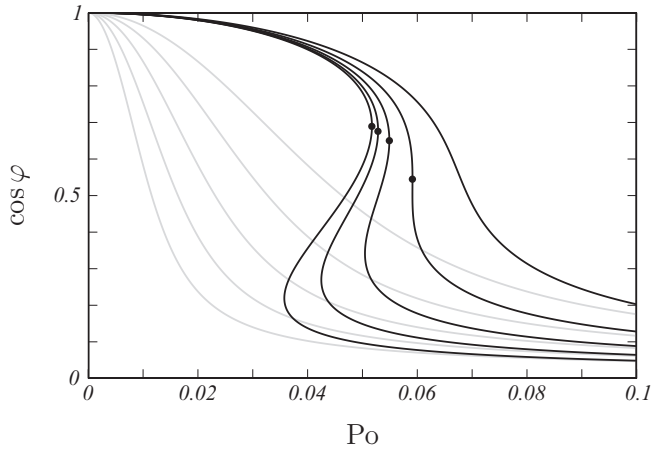

FIG. 6. The cosine of the angle φ between the axis of the spin-driven steady circulation and the spin axis as a function of Po for five different values of the Reynolds number: $\mathrm{Re} = 5\times10^3$, 10^4, 2×10^4, 4×10^4, and 8×10^4 (from right to left). We evaluate φ on the basis of Eq. (6), which is valid for steady flow in a low-Po range. Black curves, for the oblate spheroid ($\eta = 0.1$); gray curves, for a sphere. Circles on the black curves denote the points at which $d\varphi/d\mathrm{Po} = 0$.

of the angular velocity of the global circulation as

$$\omega = \cos\varphi = \frac{1}{\sqrt{1 + \mathrm{Po}^2/A}}\,, \tag{6}$$

if $\mathbf{\Omega}_s \perp \mathbf{\Omega}_p$. Here, $A(\omega; \mathrm{Re}, \eta)$ is defined by

$$A = \frac{2.62^2\,\omega}{\mathrm{Re}} + \left[\frac{0.259}{\sqrt{\mathrm{Re}\,\omega}} + \eta\,\omega^2\right]^2. \tag{7}$$

We should note that Eq. (6) holds only for steady flow, which is approximated by uniform vorticity flow except in the boundary layer, in the low-Po range ($\mathrm{Po} \ll \mathrm{Re}^{-1/2}$). However, following the argument developed by Lorenzani and Tilgner [14] and Noir *et al.* [35], we assume that the (mean) global circulation of the QT is approximately described by Eq. (6). We estimate φ, using Eq. (6), of the flow in the spheroid with $\eta = 0.1$ as a function of Po for different values of the Reynolds number: $\mathrm{Re} = 5\times10^3$, 10^4, 2×10^4, 4×10^4, and 8×10^4. The results are shown in Fig. 6 with black curves. When $\mathrm{Po} = 0$, the fluid rotates at $\mathbf{\Omega}_s$ with the container and therefore $\varphi = 0$. For each Re, as Po increases, φ also increases. Although the change of φ for $\mathrm{Re} = 5\times10^3$ is monotonic, the curves for higher Reynolds numbers ($\mathrm{Re} \gtrsim 10^4$) in Fig. 6 have turning points. The part of the curves where φ is a decreasing function ($\cos\varphi$ is an increasing function) of Po is unphysical. Therefore, we may assume that at the Poincaré number (denoted by $\mathrm{Po}^{(t)}$) where the φ has a turning point (i.e., $d\varphi/d\mathrm{Po} = 0$) the torque balance disrupts and so do the global circulation and QT [14,35,41]. It is, however, worth mentioning that in some cases of the previous study [35], which investigated parameters different from the present setup, another branch of Eq. (6) provides good prediction of the mean flow with a global circulation even for $\mathrm{Po} > \mathrm{Po}^{(t)}$. The points for the disruption are denoted by circles in Fig. 6. For $\eta = 1/10$, $\mathrm{Po}^{(t)}$ exists only for $\mathrm{Re} > 9877$, and we plot $\mathrm{Po}^{(t)}$ as a function of Re in Fig. 5 with a gray curve. This curve surprisingly coincides with the region of the hysteresis. Namely, it exists only in the Reynolds number range ($\mathrm{Re} \gtrsim 10^4$) where hysteresis exists, and the weak Re dependence of the onset of DT is also well described. Incidentally, as $A \approx \eta^2\omega^4$ for $\mathrm{Re} \gg 1$, we see that $\mathrm{Po}^{(t)} \to \eta/2$ in this limit. Therefore, if we further assume that we can apply the above argument to larger η cases, we may conclude that the range of Po for DT to be sustained is very limited for larger η. The arguments

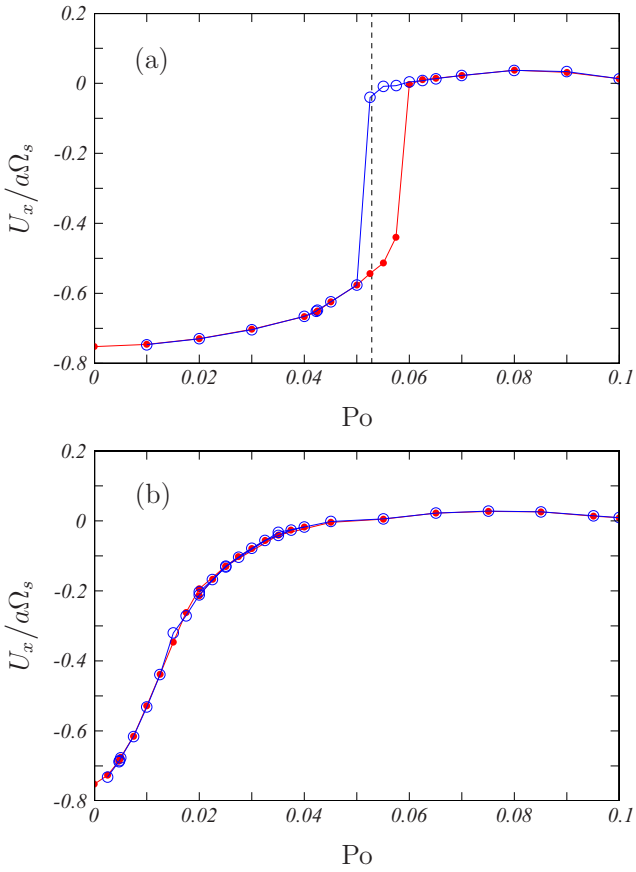

FIG. 7. The temporal average U_x of a horizontal velocity component at a point (at the distance $0.75a$ on the precession axis) shown in Figs. 4(a) and 4(b) on the equatorial plane as a function of Po. This quantity distinguishes the flow states. Namely, smaller (i.e., larger in magnitude) values of U_x correspond to QT or laminar flows, whereas the larger values correspond to DT. Red curves (with closed circles) are the results with increasing Po; blue curves (with open circles) are those with decreasing Po. (a) Results for the oblate spheroid and (b) sphere. A hysteresis loop is observed for the spheroid but not for the sphere. We fix the Reynolds number at $\mathrm{Re} = 4.0\times10^4$. In panel (a), $\mathrm{Po}^{(t)}$ ($\approx$0.0528) is indicated by the vertical dashed line.

on the basis Eq. (6) are satisfactory but not quantitatively perfect. Recall that the upper triangles in Fig. 5 denote the minimum Po for which DT is sustained when Po is decreased from a higher value (rather than the maximum Po for which QT is sustained when Po is increased from a lower value).

C. Hysteresis loop

In this subsection, we show the existence of a hysteresis loop connecting the two stable turbulent states. As observed in Figs. 4(a) and 4(b), the most remarkable difference between the two states is that the global circulation with a velocity as large as $a\Omega_s$ is dominant in the QT. We therefore adopt the temporal average U_x of the horizontal component of velocity on the equatorial plane as the indicator to distinguish the two turbulent states. Figure 7(a) shows the Po dependence of U_x, where the smaller (i.e., larger in magnitude) and larger values correspond to the QT and DT, respectively.

As described in Sec. II, after waiting for 1000 spin periods for each parameter, we measure the flow velocity for 200 spin periods to evaluate U_x. For the experiments with increasing Po, we start

with $\mathrm{Po}^{(0)} = 0$, and increase Po in a stepwise manner with an increment $\Delta\mathrm{Po} = 0.01$ for the outside of the transitional range of Po and $\Delta\mathrm{Po} = 0.0025$ in the transitional range. The results are shown with closed circles. The value of U_x suddenly increases at a value $\mathrm{Po} \in [0.0575, 0.06]$. For the experiments with decreasing Po, we start with $\mathrm{Po}^{(0)} = 0.1$, and conduct experiments with the similar procedure with increments $\Delta\mathrm{Po} = -0.01$ and -0.0025 for nontransitional and transitional ranges of Po, respectively. The results are shown with open circles in Fig. 7(a). We can observe hysteresis. Namely, in the experiments with decreasing Po, the value of U_x jumps at a value $\mathrm{Po} \in [0.05, 0.0525]$, which is lower than the Poincaré number for the sudden increase of U_x in the experiments with increasing Po. This result is consistent with the flake visualizations (Fig. 3).

We emphasize that such hysteresis in precession-driven flows is not our discovery, although our findings strengthen previous results with quantitative evidences. Even in the pioneering study by Malkus [1], he found the hysteresis of flow states by the torque measurements of a precessing spheroid with ellipticity 0.1. The sudden disruption of the nearly uniform vorticity flow was also examined by DNS with hyperviscosity by Lorenzani and Tilgner [14] for the flow in a precessing spheroidal shell under similar parameters to Malkus's experiment [1]. It was also recently reported by Herault *et al.* [28] that a hysteresis loop exists in a precessing cylinder with the aspect ratio of the diameter to the height being unity. They also showed transient turbulence in a range of Po which suddenly laminarizes without memory. Concerning transient turbulence, we have repeated the experiments described above and there seem to exist the upper and lower bounds of Po for the bistable turbulent states. Although we cannot exclude the possibility that the results depend on the waiting time, it is unrealistic to conduct experiments with longer waiting times because our waiting time is 1000 spin periods, which corresponds to about 20 min in our experimental setup for $\mathrm{Re} = 4.0\times10^4$. Incidentally, it is an interesting future study to investigate the statistics of the lifetime of the transient states just below or above the bounds so that we can unambiguously determine the lower and upper bounds of the bistable states.

D. Flow transition in a sphere

We have shown that there exist bistable turbulent states in the transitional regime of the Poincaré number between unsteady flow and developed turbulence in the oblate spheroid (with the ellipticity $\eta = 0.1$). The DT in the spheroid requires a precession with $\mathrm{Po} \gtrsim 0.05$ for the examined Re, and the QT is relatively robust in the transitional regime.

It is important to compare the above results with flow transition in a precessing sphere because, as shown below, the DT [Fig. 3(b)] is quite similar to the DT in the precessing sphere. The flake visualizations of flow in the sphere are shown in Fig. 8 for the fixed Reynolds number at $\mathrm{Re} = 4.0\times10^4$. Recall that the critical Poincaré number $\mathrm{Po}^{(c)}$ for the instability of the steady flow in the low-Po regime is given by Eq. (4) to see that unsteady flow is sustained with very weak precession of $\mathrm{Po} \approx 0.005$. As gradually increasing Po, the flow state changes continuously. The flow (for $\mathrm{Po} = 0.02$) shown in Fig. 8(a) is turbulence but it is dominated by the global circulation. This state is similar to the QT observed in the oblate spheroid. For higher Po [see Fig. 8(b) for $\mathrm{Po} = 0.024$ and Fig. 8(c) for 0.028], flow in the central region of the sphere is quiescent without small-scale turbulent eddies (see also the Supplemental Material [38]), while in an outer region flow becomes developed turbulence with small-scale structures. For further higher Po [Fig. 8(d) for $\mathrm{Po} = 0.032$], the flow is turbulent in the entire region in the sphere. We carefully conduct these experiments but do not find any discontinuous flow transition which was observed for the flow in the spheroid.

To quantitatively verify the continuity of the transition in the precessing sphere, we plot in Fig. 7(b) the value of U_x for the sphere. The results of the experiments with increasing Po are plotted with closed circles. We do not observe any discontinuity of U_x from a small value corresponding to the QT to larger values for the DT. The results of the experiments with decreasing Po are shown with open circles. These values of U_x coincide with those for the experiments with increasing Po and there is no discontinuity in U_x. This verifies the observation in Fig. 8 that there is no hysteresis of flow states in the precessing sphere. Incidentally, applying Busse's theory [36] to the sphere, we can

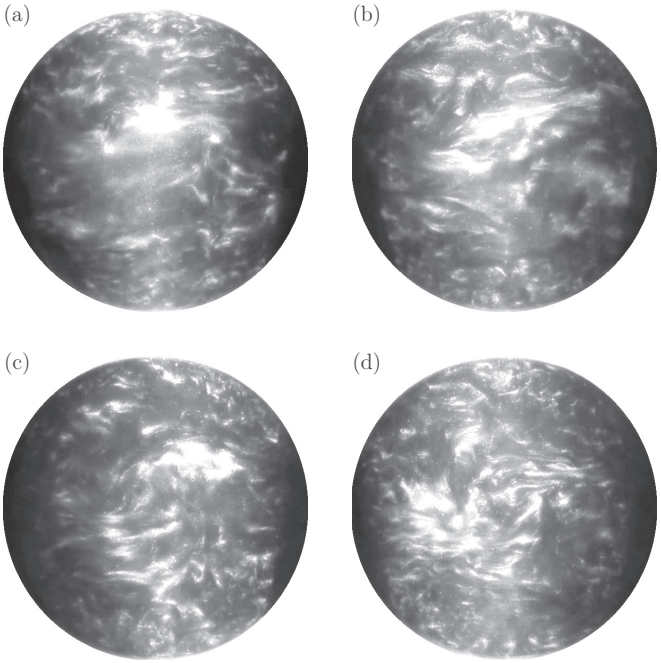

FIG. 8. Flake visualization of flow in a precessing sphere. The Reynolds number is fixed at $\mathrm{Re} = 4.0\times10^4$ and the Poincaré number is gradually increased as (a) $\mathrm{Po} = 0.02$, (b) 0.024, (c) 0.028, and (d) 0.032. Movies are available in the Supplemental Material [38].

show that there is no singular behavior of the angle φ of the inclination of the spin-driven global circulation with respect to the rotation of the spherical cavity (see the gray curves in Fig. 6). This is also consistent with the fact that turbulent states continuously change in the sphere.

For quantitative comparison, we conduct PIV for the developed turbulence in the sphere for $\mathrm{Po} = 0.055$ and $\mathrm{Re} = 4.0\times10^4$. The result is shown in Fig. 9(b) to compare with the mean velocity field of the DT in the spheroid for $\mathrm{Po} = 0.07$ ($>\mathrm{Po}^{(t)}$) [Fig. 9(a)]. These figures show that the mean flow of the DTs in the two cavities is almost identical. We emphasize again that the mean flow of the DT in the precessing sphere is complex and it is not accompanied by any global circulation [20].

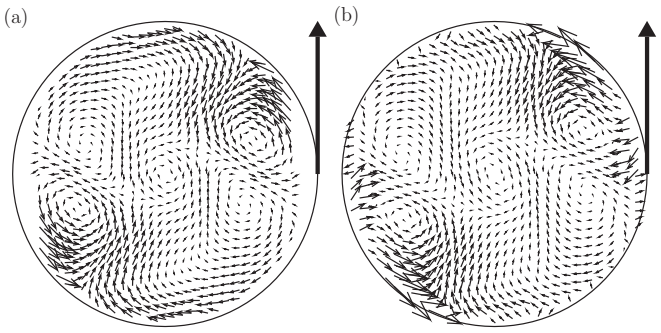

FIG. 9. Mean velocity field in (a) the oblate spheroid ($\eta = 0.1$, $\mathrm{Po} = 0.07$) and (b) a sphere ($\mathrm{Po} = 0.055$). The Reynolds number is common ($\mathrm{Re} = 4.0\times10^4$). The mean flow structures look very similar to each other despite the difference of cavity shapes. Vertical thick arrows indicate the wall speed ($a\Omega_s$) on the equatorial plane.

This implies that the mean flow of the DT in the spheroid is far from a simple global circulation. In other words, the DT in the spheroid cannot be approximated by disturbed uniform vorticity flow which is described by Eq. (6). It is important to emphasize that although the small difference of the cavity shape has significant effect on the route to the DT, the flow structures of the sustained DT are almost identical in these two cavities.

The Poincaré number for which developed turbulence in the sphere [Fig. 8(d)] is sustained is as small as 0.03. Recall that for this Po, a steady flow with the spin-driven global circulation is sustained in the spheroid with $\eta = 0.1$; see Eq. (5). These results imply that the small ellipticity significantly affects the precession-driven flow. It was shown by Busse [36] that a small ellipticity significantly weakened the differential rotation between the internal flow and cavity wall. This is because an asymmetric cavity can keep the spin-driven global circulation about an axis inclined from the spin axis due to the wall-normal stress and it is the reason why the transition from steady to unsteady flows in an asymmetric cavity requires much higher Po than in a sphere. Similarly, the ellipticity delays the transition from the QT with the spin-driven global circulation to the DT in which the global circulation is absent.

IV. CONCLUSIONS

A small change of the shape of a precessing cavity can significantly affect the flow transition of the flow of the confined fluid. We have experimentally investigated the transition to turbulence in the precessing spheroid (Fig. 1) with ellipticity $\eta = 0.1$. When we fix Re and increase Po, bistable turbulent states (Figs. 3 and 4) exist in the range of Po shown in Fig. 5. These states are substantially different from each other. Namely, one is quiescent turbulence (QT) which is accompanied by a spin-driven global circulation and the other is fully developed turbulence (DT) with nontrivial large-scale coherent vortices and small-scale turbulent eddies. The DT emerges through a subcritical transition, and the two states are connected by a hysteresis loop [Fig. 7(a)]. In contrast, such hysteresis or bistable states are not observed in the flow in the precessing sphere [Fig. 7(b)]. Despite the significant difference of the route to fully developed turbulence in the spheroid and sphere, the flow structures of the DT in these cavities are almost identical (Fig. 9).

The sudden appearance of developed turbulence for a fixed Re and increasing Po, which is demonstrated in the present study and Ref. [1] for spheroids, in Ref. [14] for a spheroidal shell, and in Refs. [6,28] for precessing cylinders, seems a feature of asymmetric cavities. This can be understood by recalling that the QT is dominated by the spin-driven global circulation. The axis of the global circulation is inclined from the spin axis due to the Coriolis force. This angle of the inclination is important to describe the flow transition in a low-Po range not only because the growth rate of the instability of steady flow in the range depends on it (see Refs. [18,37] and references therein), but also because the sudden disruption of the QT corresponds to the singular behavior of the inclination angle [14,35]. In fact, Fig. 5 shows that the value, calculated by using Busse's theory [36], of Po at which $d\varphi/d\mathrm{Po}$ becomes zero (i.e., the points shown with black circles in Fig. 6) approximately coincides with Po for the sudden disruption of the QT. As shown by the viscous solution [36] and even by the inviscid solution by Poincaré [42], a small ellipticity makes the angle of the inclination much smaller due to the wall-normal stress. It is this fact which explains the observation that the small ellipticity stabilizes the QT.

The present results (Figs. 5 and 7) of the Poincaré number range for DT is suggestive, because they imply that more symmetric container is much more effective to sustain DT and the range for the DT to be sustained in an asymmetric container is rather limited even for high Re. Recall that the analysis (Sec. III B) on the basis of Busse's theory [36] suggests that the DT is sustainable only for $\mathrm{Po} > \eta/2$, where η is the ellipticity, and, on the other hand, turbulence is drastically reduced when $\mathrm{Po} \gtrsim 0.2$ because of the steady rotation $\mathbf{\Omega}_p$ of the system. We emphasize that the fact that a small ellipticity significantly affects turbulence is crucial for engineering applications as well as geophysics. It is therefore important to show how such a qualitative change of the transition to developed turbulence appears when changing the ellipticity from zero. Although Busse's theory [14,35,36] for steady flow

in the low-Po range roughly explains the existence of the hysteresis, more quantitative investigations would be a near-future target of DNS studies.

We have successfully drawn the route to steady flow to developed turbulence in the precessing spheroid and sphere. The steady uniform vorticity flow becomes unstable due to a parametric instability [18,37] of inertial modes, and the QT stems from the nonlinear interactions of these inertial modes. Incidentally, we can observe a kind of the so-called resonant collapse to the QT in a precessing sphere (see Fig. 13 of Ref. [24]) when we suddenly impose the precession on the solid-body rotation flow. However, the physical origin of the DT sustained for Po $= O(0.1)$ is still unknown. A difficulty in solving this problem stems from the difficulty in understanding the mechanism for the nontrivial large-scale coherent vortices [Figs. 4(b) and 9, for example] to be sustained. As shown in the present paper, the DT emerges through a subcritical transition in the spheroid. This implies that we cannot reveal the origin of the DT by investigating flows in a low-Po range. Our flow visualizations suggest that the DT is continuously connected with the flows at higher Po, which tend to a solid-body rotation about the precession axis. It may be therefore interesting to investigate the flow transition from higher Po so that we can understand the origin of the DT. Besides, it is also interesting to explore the feature of the subcritical transitions in this well-controlled flow system, since nonlinear stability analysis is still a challenging problem in the research of laminar-turbulent transitions.

ACKNOWLEDGMENT

This study was partly supported by JSPS Grants-in-Aid for Scientific Research (No. 24360071 and No. 16H04268).

[1] W. V. R. Malkus, Precession of the earth as the cause of geomagnetism, Science **160**, 259 (1968).
[2] J. P. Vanyo and P. W. Linkins, Measurement of energy dissipation in a liquid-filled, precessing, spherical cavity, J. Appl. Mech. **38**, 674 (1971).
[3] J. P. Vanyo and P. W. Linkins, Rigid-body approximations to turbulent motion in a liquid-filled, precessing, spherical cavity, J. Appl. Mech. **39**, 18 (1972).
[4] J. P. Vanyo, An energy assessment for liquids in a filled precessing spherical cavity, J. Appl. Mech. **40**, 851 (1973).
[5] J. Vanyo, P. Wilde, P. Cardin, and P. Olson, Experiments on precessing flows in the earth's liquid core, Geophys. J. Int. **121**, 136 (1995).
[6] R. Manasseh, Breakdown regimes of inertia waves in a precessing cylinder, J. Fluid Mech. **243**, 261 (1992).
[7] R. Manasseh, Nonlinear behavior of contained inertia waves, J. Fluid Mech. **315**, 151 (1996).
[8] J. J. Kobine, Inertial wave dynamics in a rotating and precessing cylinder, J. Fluid Mech. **303**, 233 (1995).
[9] J. J. Kobine, Azimuthal flow associated with inertial wave resonance in a precessing cylinder, J. Fluid Mech. **319**, 387 (1996).
[10] M. Le Bars, D. Cébron, and P. Le Gal, Flows driven by libration, precession, and tides, Ann. Rev. Fluid Mech. **47**, 163 (2015).
[11] R. R. Kerswell, Upper bounds on the energy dissipation in turbulent precession, J. Fluid Mech. **321**, 335 (1996).
[12] A. Tilgner, Precession driven dynamos, Phys. Fluids **17**, 034104 (2005).
[13] A. Tilgner, Kinematic dynamos with precession driven flow in a sphere, Geophys. Astrophys. Fluid Dyn. **101**, 1 (2007).
[14] S. Lorenzani and A. Tilgner, Inertial instabilities of fluid flow in precessing spheroidal shells, J. Fluid Mech. **492**, 363 (2003).
[15] R. Hollerbach, C. Nore, P. Marti, S. Vantieghem, F. Luddens, and J. Léorat, Parity-breaking flows in precessing spherical containers, Phys. Rev. E **87**, 053020 (2013).
[16] L. Cappanera, J.-L. Guermond, J. Léorat, and C. Nore, Two spinning ways for precession dynamo, Phys. Rev. E **93**, 043113 (2016).

[17] S. Kida and M. Shimizu, A turbulent ring and dynamo in a precessing sphere, J. Phys.: Conf. Ser. **318**, 072031 (2011).
[18] Y. Lin, P. Marti, and J. Noir, Shear-driven parametric instability in a precessing sphere, Phys. Fluids **27**, 046601 (2015).
[19] Y. Lin, P. Marti, J. Noir, and A. Jackshon, Precession-driven dynamos in a full sphere and the role of large scale cyclonic vortices, Phys. Fluids **28**, 066601 (2016).
[20] S. Goto, M. Shimizu, and G. Kawahara, Turbulent mixing in a precessing sphere, Phys. Fluids **26**, 115106 (2014).
[21] C. Nore, J. Léorat, J.-L. Guermond, and F. Luddens, Nonlinear dynamo action in a precessing cylindrical container, Phys. Rev. E **84**, 016317 (2011).
[22] W. Mouhali, T. Lehner, J. Léorat, and R. Vitry, Evidence for a cyclonic regime in a precessing cylindrical container, Exp. Fluids **53**, 1693 (2012).
[23] S. Goto, N. Ishii, S. Kida, and M. Nishioka, Turbulence generator using a precessing sphere, Phys. Fluids **19**, 061705 (2007).
[24] S. Goto, A. Matsunaga, M. Fujiwara, M. Nishioka, S. Kida, M. Yamato, and S. Tsuda, Turbulence driven by precession in spherical and slightly elongated spheroidal cavities, Phys. Fluids **26**, 055107 (2014).
[25] Y. Horimoto and S. Goto, Sustaining mechanism of small-scale turbulent eddies in a precessing sphere, Phys. Rev. Fluids **2**, 114603 (2017).
[26] F. Stefani, S. Eckert, G. Gerbeth, A. Giesecke, T. Gundrum, C. Steglich, T. Weier, and B. Wustmann, Dresdyn—a new facility for MHD experiments with liquid sodium, Magnetohydrodynamics **48**, 103 (2012).
[27] F. Stefani, T. Albrecht, G. Gerbeth, A. Giesecke, T. Gundrum, J. Herault, C. Nore, and C. Steglich, Towards a precession driven dynamo experiment, Magnetohydrodynamics **51**, 275 (2015).
[28] J. Herault, T. Gundrum, A. Giesecke, and F. Stefani, Subcritical transition to turbulence of a precessing flow in a cylindrical vessel, Phys. Fluids **27**, 124102 (2015).
[29] Y. Horimoto, A. Katayama, and S. Goto, Conical shear-driven parametric instability of steady flow in precessing spheroids (unpublished).
[30] K. Avila, D. Moxey, A. de Lozar, M. Avila, D. Barkley, and B. Hof, The onset of turbulence in pipe flow, Science **333**, 192 (2011).
[31] S. G. Huisman, R. C. A. van der Veen, C. Sun, and D. Lohse, Multiple states in highly turbulent Taylor-Couette flow, Nat. Commun. **5**, 3820 (2014).
[32] R. C. A. van der Veen, S. G. Huisman, O.-Y. Dung, H. L. Tang, C. Sun, and D. Lohse, Exploring the phase space of multiple states in highly turbulent Taylor-Couette flow, Phys. Rev. Fluids **1**, 024401 (2016).
[33] D. S. Zimmerman, S. A. Triana, and D. P. Lathrop, Bi-stability in turbulent, rotating spherical Couette flow, Phys. Fluids **23**, 065104 (2011).
[34] N. Yokoyama and M. Takaoka, Hysteretic transitions between quasi-two-dimensional flow and three-dimensional flow in forced rotating turbulence, Phys. Rev. Fluids **2**, 092602(R) (2017).
[35] J. Noir, P. Cardin, D. Jault, and J.-P. Masson, Experimental evidence of nonlinear resonance effects between retrograde precession and the tilt-over mode within a spheroid, Geophys. J. Int. **154**, 407 (2003).
[36] F. H. Busse, Steady fluid flow in a precessing spheroidal shell, J. Fluid Mech. **33**, 739 (1968).
[37] R. R. Kerswell, The instability of precession flow, Geophys. Astrophys. Fluid Dyn. **72**, 107 (1993).
[38] See Supplemental Material at http://link.aps.org/supplemental/10.1103/PhysRevFluids.3.044603 for Figs. 3 and 8. For Fig. 3, Fig_3.avi shows (a) the quiescent turbulence (QT) and (b) the developed turbulence (DT) in the spheroid ($\mathrm{Re} = 4.0\times10^4$ and $\mathrm{Po} = 0055$). For Fig. 8, Fig_8.avi shows turbulent states at $\mathrm{Re} = 4.0\times10^4$ in the sphere for (a) $\mathrm{Po} = 0.02$, (b) 0.024, (c) 0.028, and (d) 0.032.
[39] D. Cébron, M. Le Bars, and P. Meunier, Tilt-over mode in a precessing triaxial ellipsoid, Phys. Fluids **22**, 116601 (2010).
[40] J. Noir and D. Cébron, Precession-driven flows in non-axisymmetric ellipsoids, J. Fluid Mech. **737**, 412 (2013).
[41] D. Cébron, Bistable flows in precessing spheroids, Fluid Dyn. Res. **47**, 025504 (2015).
[42] H. Poincaré, Sur la précession des corps déformables, Bull. Astron. **27**, 321 (1910).